Available online at www.sciencedirect.com
SCIENCE DIRECT
Solid State Communications 139 (2006) 148–152
solid state communications
www.elsevier.com/locate/ssc

Size effects on Debye temperature, Einstein temperature, and volume thermal expansion coefficient of nanocrystals

C.C. Yang[a,b], M.X. Xiao[a,b], W. Li[c], Q. Jiang[a,b,*]

[a] *Key Laboratory of Automobile Materials (Jilin University), Ministry of Education, Changchun 130022, China*
[b] *Department of Materials Science and Engineering, Jilin University, Changchun 130022, China*
[c] *Department of Mechanical Engineering, University of Alberta, Edmonton, AB, T6G 2G8, Canada*

Received 18 January 2006; received in revised form 5 May 2006; accepted 28 May 2006 by B.-F. Zhu
Available online 15 June 2006

Abstract

Based on a size-dependent root of mean square amplitude (rms) model, the size-dependent Debye temperatures of nanocrystals are modeled without any adjustable parameter by considering both Lindemann's criterion and Mott's equation. In terms of this model, the Debye temperatures depend on both size and interface conditions, which lead to related applications on size effects of the Einstein temperature and the volume thermal expansion coefficient. It is found that the model's predictions are in good agreement with available experimental and computer simulation results.

PACS: 61.46.+w; 65.40.-b

Keywords: A. Metals; D. Thermodynamic properties

1. Introduction

The physical properties of nanocrystals have been investigated extensively both theoretically and experimentally due to their scientific and industrial importance [1]. As the size of low-dimensional materials decreases to the nanometer size range, the electronic, magnetic, optic, catalytic, and thermodynamic properties of the materials are significantly altered from those of either the bulk or a single molecule [1]. Among these properties of nanocrystals, the Debye temperature of nanocrystals, $\Theta_D(D)$, has received considerable attention, since it is an essential physical quantity to characterize many material properties, such as the thermal vibration of atoms and phase transitions, where D denotes the diameter of nanoparticles and nanowires or the thickness of thin films [2–12]. Moreover, some important physical properties and their size effects, such as the Einstein temperature $\Theta_E(D)$ and the volume thermal expansion coefficient $\alpha_v(D)$, are all related to the $\Theta_D(D)$ function [4,7,13]. Once the $\Theta_D(D)$ function is known, the other two can be determined. Therefore, it is important to determine this function.

It is now known that the above physical properties of a free nanocrystal decrease as its D decreases [2,7,9,13], while they can decrease or increase for nanocrystals embedded in a matrix or deposited on a substrate [3–6,8,10–12]. A body of evidence shows that enhancement or depression of the foregoing physical properties of nanocrystals in a matrix essentially depends on the chemical interaction at interfaces between embedded nanocrystals and the matrix [3–6,8,10–12]. For instance, when the interfaces are coherent or semi-coherent, which denotes a strong bond connection, the enhancement of Θ_D of the nanocrystals is present [11,12]. Although size effects on all of the above physical properties have been modeled separately by a series of related theoretical approaches, consistent insight and a systematic thermodynamic treatment considering both the size and interface effects are highly desirable in order to reveal the physical nature of the nanocrystals.

In this contribution, $\Theta_D(D)$ functions of nanocrystals are modeled in the form of the root of mean square amplitude (rms) model. The model that is established is extended to predict the size effects on Θ_E and α_v of nanocrystals. The model

* Corresponding author at: Department of Materials Science and Engineering, Jilin University at Nanling Campus, Renmin Street, 5988, Changchun 130022, China. Tel.: +86 431 5095371; fax: +86 431 5095876.
E-mail address: jiangq@jlu.edu.cn (Q. Jiang).

0038-1098/$ - see front matter
doi:10.1016/j.ssc.2006.05.035

predictions agree well with known experimental and computer simulation results.

2. Model

In terms of the Debye model, the Θ_D function is related to the rms σ by [4,14],

$$\sigma^2 \propto T/\Theta_D^2 \tag{1}$$

when $T > \Theta_D(\infty)/2$, where T is the temperature and ∞ denotes the bulk size.

According to Lindemann's criterion [15] for melting and Mott's equation [16,17], the size-dependent rms $\sigma(D)$ has been found to have the following form [14,18]:

$$\sigma(D)/\sigma(\infty) = \sqrt{\exp\{(\alpha-1)/[(D/D_0)-1]\}} \tag{2}$$

where $\alpha = \sigma_s^2(D)/\sigma_v^2(D)$, with $\sigma_s(D)$ and $\sigma_v(D)$ denoting size-dependent rms values of the surface and interior atoms of nanocrystals, respectively [14,18], and D_0 shows a critical diameter at which all atoms of a low-dimensional material are located on its surface, which depends on dimension d and atomic diameter h through [14,19],

$$D_0 = 2(3-d)h \tag{3}$$

where $d = 0$ for nanoparticles, $d = 1$ for nanowires, and $d = 2$ for thin films.

In Eq. (2), the parameter α must be known to determine $\sigma(D)$. For crystals with free surfaces, such as free-standing particles, particles or thin films deposited on inert substrates, and nanowires in inert porous glasses, their $\sigma_s^2(D) > \sigma_v^2(D)$ and $\alpha > 1$ [14], and [14,19],

$$\alpha = [2\Delta S_{\rm vib}(\infty)/(3R)] + 1, \tag{4}$$

where R is the ideal gas constant and $\Delta S_{\rm vib}(\infty)$ is the vibrational part of the overall melting entropy $\Delta S_m(\infty)$, which consists of at least three components: positional $\Delta S_{\rm pos}(\infty)$, vibrational $\Delta S_{\rm vib}(\infty)$, and electronic $\Delta S_{\rm el}(\infty)$ [17]. Namely, $\Delta S_m(\infty) = \Delta S_{\rm vib}(\infty) + \Delta S_{\rm pos}(\infty) + \Delta S_{\rm el}(\infty)$ and $\Delta S_{\rm pos}(\infty) = -R(x_A \ln x_A + x_B \ln x_B)$, where x_A and x_B are molar fractions of crystals and vacancies, respectively [17]. For the melting transition, $x_A = 1/(1 + \Delta V_m/V_s)$, $x_B = 1 - x_A$, where $\Delta V_m = V_l - V_s$, with V being the molar volume and the subscripts s and l denoting the crystal and the liquid, respectively. For metallic crystals, the type of chemical connection does not vary during the melting transition. Thus, $\Delta S_{\rm el}(\infty) \approx 0$ [17] and $\Delta S_{\rm vib}(\infty) = \Delta S_m(\infty) - \Delta S_{\rm pos}(\infty)$, or

$$\Delta S_{\rm vib}(\infty) = \Delta S_m(\infty) + R(x_A \ln x_A + x_B \ln x_B). \tag{5}$$

However, for semi-metals, $\Delta S_{\rm el}(\infty)$ strongly contributes to $\Delta S_m(\infty)$. In this situation, $\Delta S_{\rm vib}(\infty)$ is determined by Mott's equation [16],

$$\Delta S_{\rm vib}(\infty) = 3R \ln(\nu_s/\nu_l) = (3/2)R \ln(c_s/c_l) \tag{6}$$

where ν and c denote the characteristic vibration frequency and electrical conductivity, respectively.

For nanocrystals embedded in a matrix with a coherent or semi-coherent interface, their $\sigma_s^2(D) < \sigma_v^2(D)$ and $\alpha < 1$ [19], and [19],

$$\alpha = [(h_M/h)^2 T_m(\infty)/T_M(\infty) + 1]/2, \tag{7}$$

where h_M denotes the atomic diameter of the matrix, and $T_m(\infty)$ and $T_M(\infty)$ are the bulk melting temperature of the nanocrystals and the matrix, respectively.

Based on Eq. (1), it is assumed that $\Theta_D(D)$ has the same size dependence of $1/\sigma(D)$ as a first-order approximation, since the nature of any phase transition is related to the potentials of the two related phases of the crystals. Thus,

$$\Theta_D(D)/\Theta_D(\infty) = \sigma(\infty)/\sigma(D). \tag{8}$$

Substituting Eq. (2) into Eq. (8), this reads,

$$\Theta_D(D)/\Theta_D(\infty) = \sqrt{\exp\{-(\alpha-1)/[(D/D_0)-1]\}}. \tag{9}$$

Since $\Theta_E(\infty) \propto \Theta_D(\infty)$ [4] and $\alpha_v(\infty) \propto 1/\Theta_D^2(\infty)$ [7], Eq. (9) can be extended for $\Theta_E(D)$ and $\alpha_v(D)$ functions as follows:

$$\Theta_E(D)/\Theta_E(\infty) = \sqrt{\exp\{-(\alpha-1)/[(D/D_0)-1]\}}, \tag{10}$$

$$\alpha_v(D)/\alpha_v(\infty) = \exp\{(\alpha-1)/[(D/D_0)-1]\}. \tag{11}$$

3. Results and discussion

Comparisons between model predictions in terms of Eqs. (4), (7) and (9) and the available experimental and computer simulation results for $\Theta_D(D)$ functions of Fe, β-Sn, Se, Cu, Co, Au, and Ar/Al (Ar nanocrystals embedded in Al matrix) nanocrystals are shown in Fig. 1, where the related parameters are listed in Table 1 (parameters used for other figures are also listed in this table). It is obvious that our model predictions for different kinds of nanocrystals in different surroundings correspond to the experimental and computer simulation results in the full size range, which implies that Eq. (9) is reasonable.

As shown in Fig. 1(a)–(f), $\Theta_D(D)$ with $\alpha > 1$ decreases for free nanocrystals as D decreases. $\alpha > 1$ implies a decrease in $\Theta_D(D)$ with an increase in the rms. Note that Fe and β-Sn films in Fig. 1(a) and (b) may refer to fine granular structures with high densities of inner surface/grain boundaries and cannot be described by a continuous film [14]. This granular structure is similar to a random structure of a chain polymer, modeled by the trajectory of a self-avoiding walk with a fractal dimension of $d = 4/3$ [14]. It is obvious that the depression for $\Theta_D(D)$ of films with D is weaker than that of nanoparticles, as shown in Fig. 1(a) and (b), which is induced by different values of d and thus different values of D_0 in Eq. (3). Consequently, our model can also predict the dimension dependence of $\Theta_D(D)$, while different dimensions of nanocrystals have different surface/volume ratios.

For nanocrystals embedded in a matrix with a coherent or semi-coherent interface, such as the Ar/Al system in Fig. 1(g), $\Theta_D(D)$ with $\alpha < 1$ increases as D decreases. $\alpha < 1$ implies the suppression of the rms of the nanoparticles

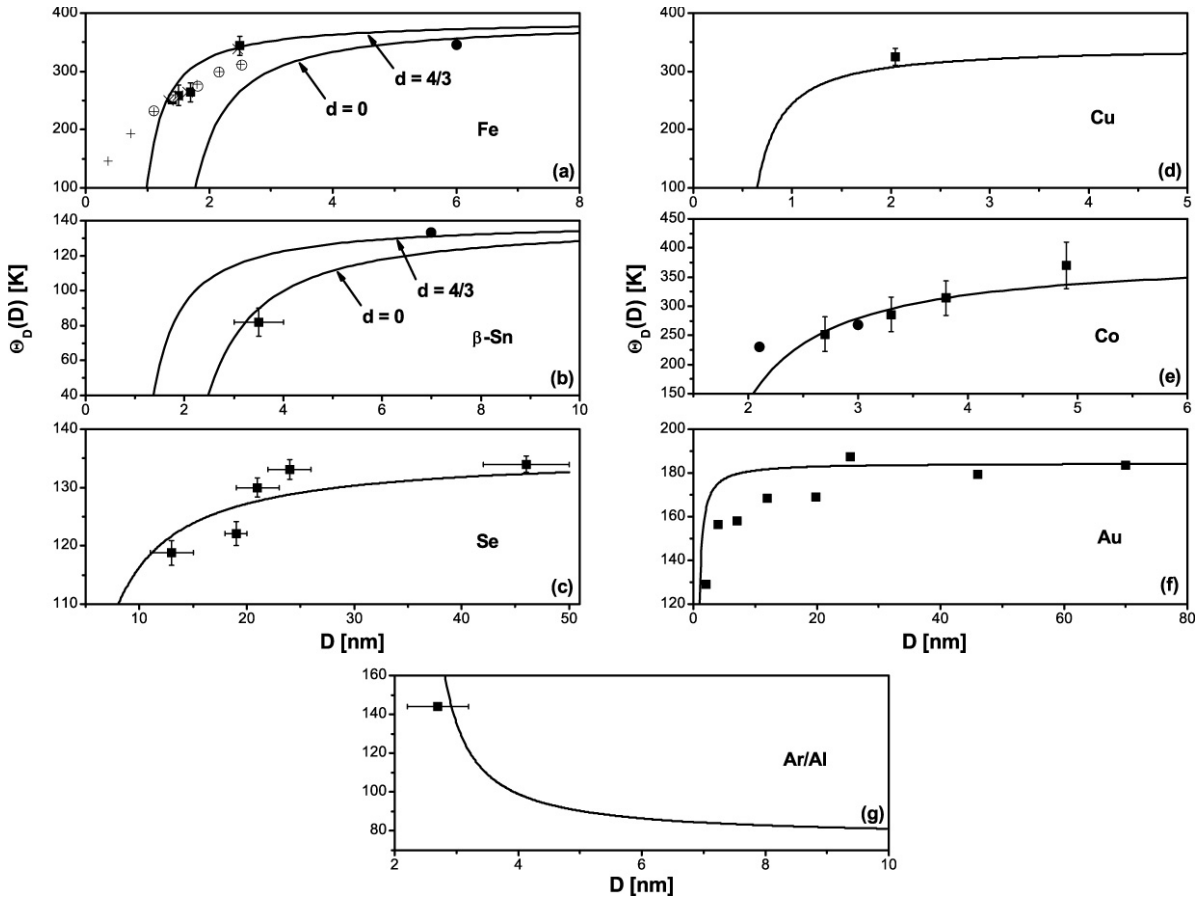

Fig. 1. $\Theta_D(D)$ functions of Fe, β-Sn, Se, Cu, Co, Au, and Ar/Al (Ar nanocrystals embedded in Al matrix). The solid lines in (a)–(f) denote the model predictions in terms of Eqs. (4) and (9), while in (g) they denote the model predictions based on Eqs. (7) and (9) and D_0 is determined by Eq. (3). (a) The symbols ● (nanoparticles, $d = 0$) [2], × [3], + [3], ■ [4], and ○ [4] (films with fine granular structures, $d = 4/3$ [14]) show the experimental results of Fe, where the error bars are also shown (the same for the below). (b) The symbols ● (films with fine granular structures, $d = 4/3$ [14]) [5] and ■ (nanoclusters embedded in SiO_2 layers, $d = 0$) [6] show the experimental results of β-Sn. (c) The symbol ■ (nanoparticles, $d = 0$) [7] shows the experimental results of Se. (d) The symbol ■ (thin films on graphite substrate, $d = 2$) [8] shows the experimental results of Cu. (e) The symbols ■ [9] and ● [9] (nanoclusters, $d = 0$) show the experimental and computer simulation results of Co, respectively. (f) The symbol ■ (thin films on mica substrate, $d = 2$) [10] shows the experimental results of Au. (g) For the Al matrix, $h_M = 0.2863$ nm [22] and $T_M(\infty) = 933.47$ K [20]. The symbol ■ (Ar nanoparticles embedded in Al matrix, $d = 0$) [11] shows the experimental results of Ar/Al.

Table 1
Necessary parameters used to determine $\Theta_D(D)$, $\Theta_E(D)$, and $\alpha_v(D)$ functions

	$\Theta_D(\infty)$	$T_m(\infty)$ [20]	$\Delta H_m(\infty)$ [20]	$\Delta V_m/V_s$ [21] (%)	$\Delta S_{\text{vib}}(\infty)$	h [22]
Fe	388.00 [4]	1811.00	13.80	3.4	6.42[a]	0.2482
β-Sn	140.00 [6]	505.08			9.25[b]	0.3181
Se	135.90 [7]	494.00	5.40		10.93[c]	0.4366 [7]
Cu	343.00 [8]	1357.77	13.10	4.9	8.08[a]	0.2556
Co	400.00 [9]	1768.00	16.20	3.9	7.83[a]	0.2507
Au	184.59 [10]	1337.33	12.50	5.1	7.74[a]	0.2884
Ar	70.00 [11]	83.80				0.3650 [11]
Pb		600.61	4.77	3.5	6.71[a]	0.3500

$\Theta_D(\infty)$ and $T_m(\infty)$ are in K, the bulk melting enthalpy $\Delta H_m(\infty)$ in kJ mol^{-1}, $\Delta S_{\text{vib}}(\infty)$ in J mol^{-1} K^{-1}, and h is in nm.
[a] The values are calculated by Eq. (5), where $\Delta S_m(\infty) = \Delta H_m(\infty)/T_m(\infty)$ and $R = 8.314$ J mol^{-1} K^{-1}.
[b] The value is determined by Eq. (6) with $c_s/c_l = 2.10$ [17].
[c] The values are approximately equal to $\Delta S_m(\infty)$ [19].

as a total effect induced by both the surface and the interface. Although the surface of the nanocrystals still has a tendency to lower the $\Theta_D(D)$ value, the total effect of the surface and the interface between the nanocrystals and the matrix leads to a drop in the internal energy of the nanocrystals and thus an increase in $\Theta_D(D)$ as D decreases. Note also that $h_M < h$ in the system reported above, although it is not a necessary condition for $\alpha < 1$ in

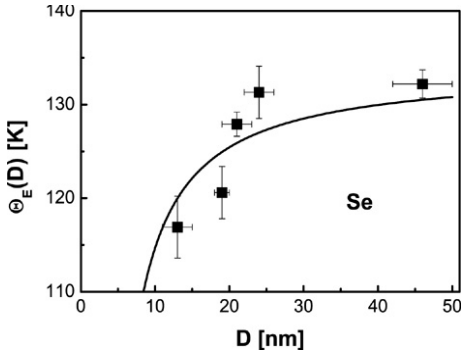

Fig. 2. $\Theta_E(D)$ function of Se. The solid line denotes the model predictions in terms of Eqs. (4) and (10), where $\Theta_E(\infty) = 134.00$ K [7], and D_0 is determined by Eq. (3). The symbol ■ (nanoparticles, $d = 0$) [7] shows the experimental results of Se.

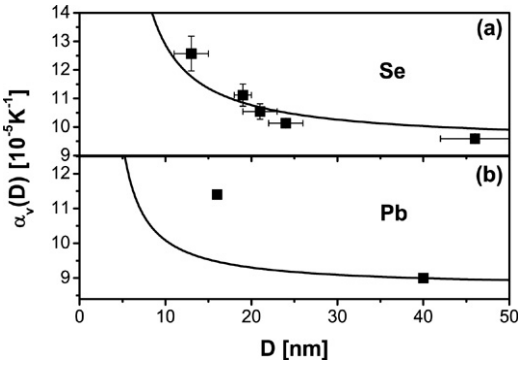

Fig. 3. $\alpha_v(D)$ functions of Se and Pb. The solid lines denote the model predictions in terms of Eqs. (4) and (11) and D_0 is determined by Eq. (3). (a) For Se, $\alpha_v(\infty) = 9.45 \times 10^{-5}$ K^{-1} is a mean value of 7.8×10^{-5} K^{-1} [7] and 11.1×10^{-5} K^{-1} [23] as a first order approximation. The symbol ■ (nanoparticles, $d = 0$) [7] shows the experimental results of Se. (b) For Pb, $\alpha_v(\infty) = 8.7 \times 10^{-5}$ K^{-1} [23]. The symbol ■ (nanoparticles, $d = 0$) [13] shows the experimental results of Pb. Note that the original experimental results is the linear expansion coefficient $\alpha_l(D)$ of Pb nanocrystals. As a first order approximation, $\alpha_v(D) = 3\alpha_l(D)$ is used [23].

Eq. (9). It is plausible that if $h_M > h$, the local internal stress at the interface is a tensile stress, which increases, but does not decrease the rms of the surface atoms of the nanocrystals. Thus, any evident enhancement of $\Theta_D(D)$ should occur under the condition $h_M < h$.

A comparison between the model predictions in the frame of Eqs. (4) and (10) and the available experimental results for the $\Theta_E(D)$ function of Se nanocrystals is shown in Fig. 2, where $\Theta_E(D)$ decreases as D drops. There are good agreements between the model predictions and the experimental evidence, although only experimental results of $\Theta_E(D)$ suppression are compared due to the unavailability of experimental evidence.

As shown in Fig. 3(a) and (b), comparisons between the model predictions based on Eqs. (4) and (11) and experimental results for $\alpha_v(D)$ of Se and Pb nanocrystals are presented. The model predictions correspond to the experimental results of Se nanocrystals over the full size range, as shown in Fig. 3(a). For Pb nanocrystals in Fig. 3(b), our model can predict the $\alpha_v(D = 40$ nm) value accurately in comparison with the experimental results, while a big divergency between them is found for the $\alpha_v(D = 16$ nm) value. One possible reason is that the approximation of $\alpha_v(D) = 3\alpha_l(D)$ could collapse in a smaller size range (such as $D = 16$ nm). As mentioned above, $\alpha_v(D)$ increases with decreasing D. It is known that $E_c \propto 1/\alpha_v$, where E_c denotes the cohesive energy of atoms [13] and $E_c(D)$ decreases with decreasing D [24], which confirms Eq. (11).

Note that, in the above consideration, the effect of size on h has been neglected, i.e. V_s or h is assumed to be a size-independent constant, namely $\Delta V_s = V_s(\infty) - V_s(D) \approx 0$ or $\Delta h = h(\infty) - h(D) \approx 0$. It is known that $\Delta h/h = \Delta V_s/(3V_s) = 0.1\%$–$2.5\%$ when $D < 20$ nm, and it is negligible when $D > 20$ nm [25]. Thus, even for $D < 20$ nm, $[V_s(D)/V_s(\infty)]^{2/3} \approx 0.95$–$0.97$. According to Lindemann's criterion, $\Theta_D = c_1[T_m/(MV_s^{2/3})]^{1/2}$ [26], where c_1 is a constant and M denotes the molar weight and is size-independent. Thus, $T_m(\infty) \propto \Theta_D^2(\infty)V_s(\infty)^{2/3}$. If $T_m(D)$ has the same size dependence of $\Theta_D^2(D)V_s(D)^{2/3}$ as a first-order approximation, $T_m(D)/T_m(\infty) = [\Theta_D^2(D)/\Theta_D^2(\infty)][V_s(D)/V_s(\infty)]^{2/3}$. Similarly, $\alpha_v(D)/\alpha_v(\infty) = [\Theta_D^2(\infty)/\Theta_D^2(D)]/[V_s(D)/V_s(\infty)]^{2/3}$, since $\Theta_D = c_2/(\alpha_v MV_s^{2/3})^{1/2}$, with c_2 being a constant [7]. Thus, the error range induced by $[V_s(D)/V_s(\infty)]^{2/3}$ is only 3%–5% for the $T_m(D)$ function in our former prediction [14,19] and for the $\alpha_v(D)$ function in the present prediction. This high-order error has also been neglected for simplicity in Ref. [18].

As shown above, $\Theta_D(D)$, $\Theta_E(D)$, and $\alpha_v(D)$ functions for different kinds of nanocrystals and different surroundings can be described as long as the related thermodynamic parameters of crystals are known. The physical nature of the enhancement or suppression of these physical properties is related to both the surface/volume ratio and the interfacial energetic change between embedded nanocrystals and the matrix.

4. Conclusions

In summary, a model for the $\Theta_D(D)$ function is established by considering both Lindemann's criterion and Mott's equation. The $\Theta_D(D)$ function decreases for free nanocrystals and increases for nanocrystals having a strong chemical interaction with their surroundings as D decreases. Since the $\Theta_E(D)$ and $\alpha_v(D)$ functions have simple relations to the $\Theta_D(D)$ function, these functions are also developed. The model's predictions correspond to known experimental and computer simulation results.

Acknowledgements

Financial support from the National Key Basic Research and Development Program (Grant No. 2004CB619301) and from the "985 Project" of Jilin University are acknowledged.

References

[1] H. Gleiter, Acta Mater. 48 (2000) 1.
[2] U. Herr, J. Jing, R. Birringer, U. Gonser, H. Gleiter, Appl. Phys. Lett. 50 (1987) 472.
[3] M.Y. Zhou, P. Sheng, Phys. Rev. B 43 (1991) 3460.
[4] J.R. Childress, C.L. Chien, M.Y. Zhou, P. Sheng, Phys. Rev. B 44 (1991) 11689.
[5] L.B. Hong, C.C. Ahn, B. Fultz, J. Mater. Res. 10 (1995) 2408.

[6] G.E.J. Koops, H. Pattyn, A. Vantomme, S. Nauwelaerts, R. Venegas, Phys. Rev. B 70 (2004) 235410.
[7] Y.H. Zhao, K. Lu, Phys. Rev. B 56 (1997) 14330.
[8] M. Kiguchi, T. Yokoyama, D. Matsumura, H. Kondoh, O. Endo, T. Ohta, Phys. Rev. B 61 (2000) 14020.
[9] M. Hou, M.E. Azzaoui, H. Pattyn, J. Verheyden, G. Koops, G. Zhang, Phys. Rev. B 62 (2000) 5117.
[10] G. Kästle, H.-G. Boyen, A. Schröder, A. Plettl, P. Ziemann, Phys. Rev. B 70 (2004) 165414.
[11] C.J. Rossouw, S.E. Donnelly, Phys. Rev. Lett. 55 (1985) 2960.
[12] L.K. Nanver, G. Weyer, B.I. Deutch, Phys. Status Solidi A 61 (1980) K29.
[13] J.-G. Lee, H. Mori, Eur. Phys. J. D 34 (2005) 227.
[14] Q. Jiang, H.Y. Tong, D.T. Hsu, K. Okuyama, F.G. Shi, Thin Solid Films 312 (1998) 357.
[15] F.A. Lindemann, Z. Phys. 11 (1910) 609.
[16] N.F. Mott, Proc. R. Soc. London, Ser. A 146 (1934) 465.
[17] A.R. Regel', V.M. Glazov, Semiconductors 29 (1995) 405.
[18] F.G. Shi, J. Mater. Res. 9 (1994) 1307.
[19] M. Zhao, Q. Jiang, Solid State Commun. 130 (2004) 37.
[20] http://www.webelements.com/.
[21] Q. Jiang, X.H. Zhou, M. Zhao, J. Chem. Phys. 117 (2002) 10269.
[22] H.W. King, in: R.W. Cahn (Ed.), Physical Metallurgy, North-Holland, Amsterdam, 1970, p. 60.
[23] R.C. Weast, CRC Handbook of Chemistry and Physics, 69th edition, CRC Press, Boca Raton, FL, 1988–1989, p. D-185, F-107.
[24] Q. Jiang, J.C. Li, B.Q. Chi, Chem. Phys. Lett. 366 (2002) 551.
[25] Q. Jiang, L.H. Liang, D.S. Zhao, J. Phys. Chem. B 105 (2001) 6275.
[26] J.G. Dash, Rev. Mod. Phys. 71 (1999) 1737.